LASER & PHOTONICS REVIEWS

Laser Photonics Rev. **8,** No. 1, 172–179 (2014) / **DOI** 10.1002/lpor.201300121

ORIGINAL PAPER

Abstract Indium Tin Oxide (ITO) coated glass is currently the preferred transparent conducting electrode (TCE) for organic light emitting diodes (OLEDs). However, ITO has its drawbacks, not least the scarcity of Indium, high processing temperatures, and inflexibility. A number of technologies have been put forward as replacements for ITO. In this paper, an OLED based on a gold grid TCE is demonstrated, the light emission through the grid is examined, and luminance and current measurements are reported. The gold grid has a sheet resistance of 15 $\Omega\square^{-1}$ and a light transmission of 63% at 550 nm, comparable to ITO, but with advantages in terms of processing conditions and cost. The gold grid OLED has a lower turn-on voltage (7.7 V versus 9.8 V) and achieves a luminance of 100 cdm^{-2} at a lower voltage (10.9 V versus 12.4 V) than the reference ITO OLED. We discuss the lower turn-on voltage and the uniformity of the light output through the gold grid TCE and examine the conduction mechanisms in the ITO and gold grid TCE OLEDs.

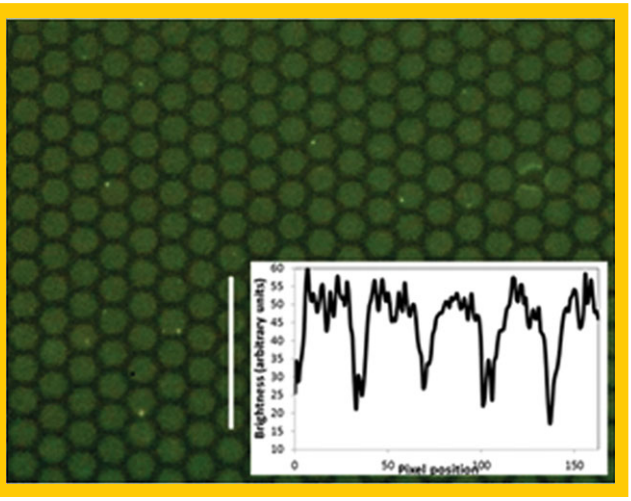

Thin film hexagonal gold grids as transparent conducting electrodes in organic light emitting diodes

F. Laurent M. Sam, Christopher A. Mills, Lynn J. Rozanski, and S. Ravi P. Silva*

1. Introduction

Organic Light Emitting Diodes (OLEDs) and Liquid Crystal Displays (LCDs) can these days be found in electronics applications such as modern mobile phones, televisions, tablet computers and personal computers. They commonly utilise a transparent conducting electrode (TCE) through which light is emitted but which must also carry charge to the emissive layer. Some of the important properties for a TCE include high transparency at the emitted wavelength of the OLED, low sheet resistance ($<20\ \Omega\square^{-1}$) and preferably a low cost [1].

ITO is currently the most popular TCE used in the electronics industry. It has excellent sheet resistance (as low as 10 $\Omega\square^{-1}$), high transmission in the visible wavelength range (typically 85% on average from 400–700 nm) and its fabrication process has been thoroughly optimised [2]. However, it has some drawbacks which limit its application in future devices. For example, ITO is brittle so it cannot be used in conjunction with flexible OLEDs [3]. Due to its relative scarcity [4], the price of indium is expected to rise, increasing the cost of production of OLEDs [5]. ITO also requires a high processing temperature, and indium migration has been shown to limit device lifetime [6, 7].

Therefore, an alternative TCE to ITO must be developed. Several solutions have been considered based on novel technologies, including the use of carbon nanotubes (CNT) [8], graphene, thin metal films (a few nanometres thick to retain transparency) [9], metal grids and silver nanowires [10, 11]. CNT and graphene have high charge carrier mobilities and their measured resistivities have been shown to be lower than metals such as gold or silver. They have a low percolation threshold, so in theory only a low concentration would be required to achieve a low sheet resistance suitable for TCEs. The low concentrations needed would imply that the light absorption of the resultant TCE would also be low. Unfortunately, the contact resistance between individual CNTs is very high and the grain boundaries in graphene present a barrier to charge conduction. This makes the sheet resistance of CNTs and graphene prohibitive for use as a TCE over a large area.

Low sheet resistances have been achieved with silver nanowires [10]. The contact resistances between individual silver nanowires can be reduced considerably by sintering. Nevertheless, the surface roughness of a film of nanowires, which is related to the diameter of the nanowires, can be on the order of 100 nm. This is relatively large and can short circuit most thin films used in optoelectronic devices. The nanowires are also heterogeneously arranged, and local sheet resistance or transmission can be worse than the calculated global optimum. Typically, thin metal films have a poor trade-off between sheet resistance and light transmission [9].

The alternatives to ITO discussed above all have their merits and disadvantages. Here we examine the applicability of thin gold grids in a hexagonal geometry for TCE

Advanced Technology Institute, University of Surrey, Guildford, GU2 7XH, UK
*Corresponding author: e-mail: s.silva@surrey.ac.uk

applications. The hexagonal grid structure has previously been used to make solar cell devices (e.g. by Galagan et al. [12] and Yu et al. [13]). The grids were printed onto flexible substrates and organic solar cells were fabricated onto the grids. In this paper, we show that OLEDs can also be made using a grid TCE. Photolithography was used to fabricate the grids with line widths were on the order of micrometres, invisible to the naked eye, so that light from the grid TCE OLED would appear as uniform as an ITO OLED. The advantage of metal grids over a nanometre thick sheet of metal is that the sheet resistance can be decreased by using a thick grid line, whilst having little effect on the light transmission [14–16]. Although metal grids can have a high surface roughness, especially if very thick line thicknesses (>30 nm) are used, this can be mitigated by planarising the surface with a transparent polymer before the OLED layers are deposited.

Our use of gold as the metal grid is purely to illustrate the applicability of metal grids as replacements to ITO, and once perfected the gold may be substituted. At present, gold is about 30 times more expensive than indium. Despite that, less gold is required, by volume, to make a TCE with an equivalent sheet resistance to ITO. The deposition of ITO is also more costly than the deposition of gold (or other metals), being as it commonly uses electron beam evaporation, or sputter deposition techniques, rather than thermal deposition. Subsequently, the preparation of a gold grid TCE and an ITO TCE cost approximately the same. Using copper for example (1/5000 of the price of gold and 150 times cheaper than indium [London Metal Exchange 29/05/13]), instead of gold, would make the metal TCE cheaper than an equivalent ITO TCE, with a similar sheet resistance. Nonetheless, price is not the only, nor the most important, issue with ITO as discussed above.

This paper demonstrates the feasibility of producing an OLED using a gold grid as the TCE, and characterises the electrical and optical properties of the fabricated device. An OLED on a Cu grid has been reported previously [17], but characterisation was limited to the examination of the IV characteristics. Here we present the one of the few luminance measurements of OLEDs on grids, and images of light emission through the grid.

2. Materials and methods

2.1. Materials

Acetone, methanol and propan-2-ol (IPA) were sourced from Sigma-Aldrich, USA and used as received. Poly(3,4-ethylenedioxythiophene) poly(styrenesulfonate) (PEDOT:PSS, Clevios PVP AI4083, solid content 1.3%, PEDOT:PSS ratio 1:6) was purchased from HC Stark, Germany, and was filtered through a 0.45 μm PTFE filter before use. Poly(9,9 '-dioctylfluorene-co-benzothiadiazole) (F8BT, ADS133YE) was sourced from American Dye Source, Canada. It was in the form of a solid powder and was dissolved in chloroform at a concentration of 5 mg/ml inside a nitrogen-filled glovebox. Patterned ITO coated glass substrates (approx. 15 $\Omega\square^{-1}$) were purchased from Luminescence Technology Corp., Taiwan.

2.2. TCE production

Glass substrates were cleaned by ultrasonication in acetone for 10 minutes followed by a plasma ash (KM1050X Plasma Etcher/Asher/Cleaner from Quorum Technologies) at 100 W for 5 minutes using an oxygen gas flow of 15 sccm. Photolithography was performed in a yellow room inside a Class 1000 cleanroom. Hexamethyldisilazane (HMDS) (Sigma-Aldrich, Germany) was first spin coated (3500 rpm for 35 seconds at maximum acceleration) on to the glass substrate to act as an adhesion promoter for the photoresist layer. This was followed by a layer of S1813 (Microposit, Dow Chemical Company, USA), spin coated with the same parameters, to give a photoresist thickness of 1.5 μm. The photoresist was then baked on a hotplate at 115 °C for 1 minute. After allowing it to return to room temperature, the photoresist was exposed using a Quintel Corporation Ultra μLine 7000 Series I-line UV mask aligner for an exposure dose of 40 mJ/cm^2. The photoresist was then developed in MF-319 developer (Microposit, Dow Chemical Company, USA) for 14 seconds. It was finally rinsed in water and blown dry with nitrogen, before inspecting with a light microscope to check the features were well defined.

Metal of the required thickness (30 nm) was sputtered onto the sample using a JLS designs MPS 500 sputter coater system. The sample was immersed in acetone overnight to allow lift-off to occur. The final step was gentle sonication in an ultrasonic water bath to remove the photoresist, after which the grid TCE could be used.

The line width of the grid was 3 μm, the line spacing was 10 μm, and the line thickness (height of the lines) was 30 nm.

2.3. OLED production

OLEDs were fabricated on the gold TCE deposited glass substrate, and on ITO coated glass. The substrates were cleaned by immersion in acetone, IPA and methanol in an ultrasonic bath for 5 min each, followed by 5 min in a plasma asher. PEDOT:PSS was deposited on the substrates by spin coating at a slow speed (2000 RPM for 1 min.). The deposition at slow spin speed produced a thick PEDOT:PSS layer (80 nm) to planarise the surface to prevent short circuits in the OLED due to the rough grid surface. Subsequent steps were performed in a nitrogen atmosphere, free of oxygen and water, inside a glovebox. After spin-coating PEDOT:PSS, the substrate was annealed at 150 °C for 10 min. under nitrogen. After cooling, F8BT was deposited by spin coating for 1 min at 1000 RPM. The F8BT was then annealed at 150 °C for 10 min. This was followed by 5 nm of 2,9-dimethyl-4,7-diphenyl-1,10-phenanthroline (Bathocuproine, or BCP) and 60 nm of aluminium which

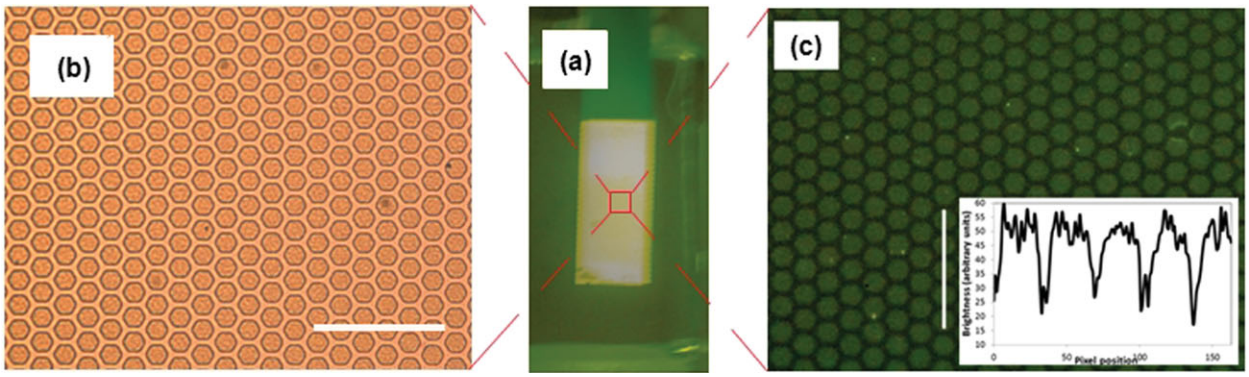

Figure 1 (a) Large scale photograph of an OLED made on a Ag grid TCE (2 mm × 4 mm); (b) optical microscope image of the Au grid TCE in the OLED in the off state [scale bar = 50 μm]; (c) optical microscope image of light emission from the OLED through the gaps in the grid (Note: the image has brightness and contrast adjusted for clarity, and that the scale bar for (b) and (c) is the same); and (inset) profile plot of the light intensity along the white line in (c). Image analysis completed using ImageJ software.

were evaporated onto the F8BT using a mask to define the OLED active area (8 mm^2). The device was encapsulated before characterisation, and stored under nitrogen in the dark.

2.4. OLED characterisation

The sheet resistance of the gold grid TCE was measured using the transmission line method [18]. A mask was designed so that 1 mm wide contacts could be deposited at 6 different line spacings. 100 nm of gold was sputtered onto the TCE through the mask and the resistance was measured across each line spacing. The resistance was plotted against the contact spacing. The gradient of the graph was divided by the length of the contacts to find the sheet resistance.

Optical transmission was measured using a UV-Visible spectrometer (Perkin-Elmer). A substrate with the TCE on it was placed inside the spectrometer with the TCE side facing the incident sample beam. The same substrate without the TCE was used for the reference beam. The measurement was taken in the wavelength range of 230 nm to 2000 nm. The transmission at a wavelength of 550 nm was chosen for comparison between TCEs as it is approximately the peak wavelength of light emission from F8BT.

3. Results and discussion

3.1. Optical properties

The Au grid TCE, fabricated on a glass substrate with dimensions of 3 μm line width, 10 μm line spacing and 30 nm line thickness (Fig. 1b), was found to have a sheet resistance of 15 $\Omega\square^{-1}$ and a transmission of 63% at a wavelength of 550 nm. For comparison, the ITO used for the reference OLED has a sheet resistance of 15 $\Omega\square^{-1}$ and a transmission of 87% at the same wavelength. The area covered by the grid lines is 44% of the total area of the substrate. The transmission of light through the grid is therefore not only through the gaps (which make up 56% of the substrate area), but also through the grid lines themselves. According to Palik [36], a 30 nm thick film of gold has a transmission of 16% which is not an insignificant amount. Some of the light passing through the grid lines could be scattered, so that less than 16% would reach the light detector after passing through the grid lines. This would account for the difference between the area not covered by the grid lines and the transmission through the TCE.

The F8BT OLED incorporating the Au grid TCE had a uniform light emission as seen in Fig. 1a. There were no dark spots, although it is possible that some defects in the grid could create dark spots on the micrometre scale. Any defects on that scale would have an almost negligible effect on the OLED light uniformity. Using a light microscope, the OLED was found to emit light through the hexagons defined by the Au grid (Fig. 1c). An imaging program (ImageJ, NIH, USA) was used to analyse the light intensity. A sectional profile of light intensity (Fig. 1c inset) shows that the light emission through the gaps is relatively uniform and that almost no light is emitted through the gold grid lines. The FWHM of the intensity peaks in the ImageJ intensity profile (inset of Fig. 1c) was found to be 10 μm. This is equal to the grid line spacing which shows that there is no difference between the line width (Fig. 1b) and the apparent shadow width of the light emission through the grid (Fig. 1c).

The optoelectronic properties of F8BT OLEDs have been compared; one with the Au grid TCE, and a reference device incorporating an ITO electrode (Fig. 2). The OLED with the Au grid TCE has a lower turn-on voltage (defined as the voltage at which the luminance equals 1 cdm^{-2}) compared to the reference ITO device (7.7 V compared to 9.8 V) as shown in Fig. 2a. This can be explained by examining the band diagram for the diodes (Fig. 2c). Holes prefer to move towards a lower (more positive) energy level when passing from the TCE to the polymers in the diode. As Au has a higher work function than ITO (−5.4 eV versus −4.7 eV), and as the HOMO (Highest Occupied Molecular Orbital) of PEDOT:PSS is −5.2 eV,

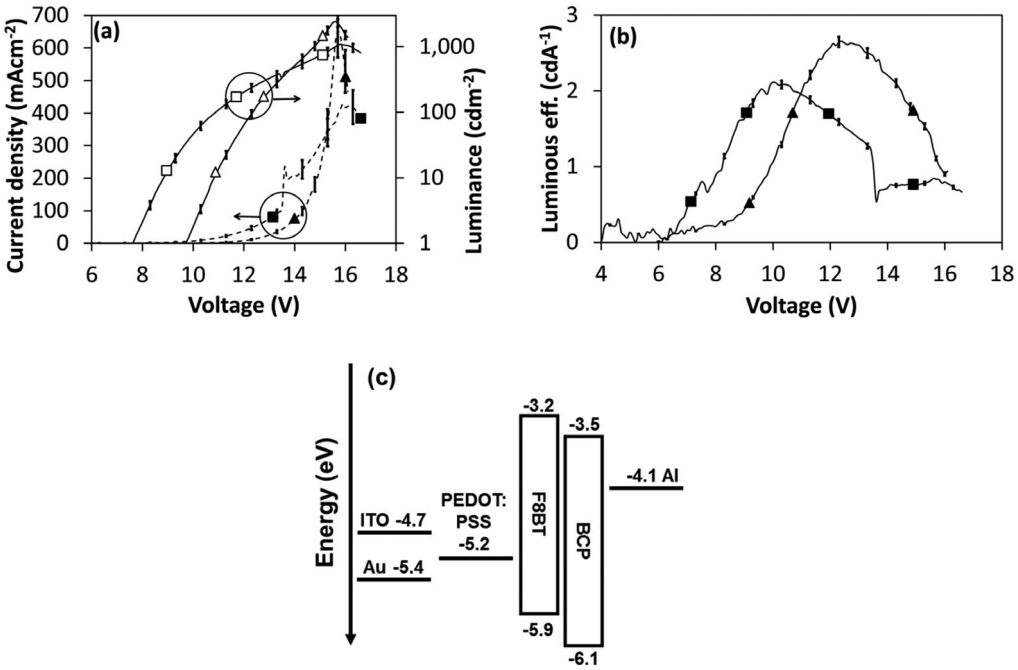

Figure 2 Plots of (a) current density (closed symbols) and luminance (open symbols), and (b) luminous efficiency, of OLEDs with a Au grid TCE (squares) and an ITO electrode (triangles). (c) Diagram depicting the energy levels of the components in the diodes prior to electrical contact [19–21]. The largest source of error came from the measurement of the size of the OLED (±12%).

this means that there is a lower energy barrier for hole injection from the Au grid anode to PEDOT:PSS, than from the ITO anode to PEDOT:PSS. In the OLED with the Au grid TCE, holes enter the diode at a lower voltage, and consequently the OLED begins to emit light at the lower voltage.

In comparison to analogous devices reported in the literature, the operating voltage of the OLEDs is quite high. An optimised F8BT OLED produced for comparison, using ITO as the transparent conductor, has a turn-on voltage of 3 V and attains a maximum luminance at 5–7 V because it uses a thinner PEDOT:PSS layer. The thick layer of PEDOT:PSS used here was necessary because of the rough surface of the grid electrode. For a direct comparison with the Au TCE OLED, the ITO OLED used here incorporates the same PEDOT:PSS thickness as the TCE OLED, and consequently also displays a high operating voltage. If a method for planarising the surface of the gold TCE is used (e.g. by burying the Au grid in the substrate), the PEDOT:PSS layer can be thinner, reducing the operating voltage to a level comparable with the optimised ITO device.

The reference ITO OLED achieves a maximum luminance of 2410 cdm^{-2} at 15.6 V, whilst the Au grid TCE OLED reaches a maximum luminance of 1050 cdm^{-2} at 15.7 V. This is about 45% of the maximum luminance of the reference OLED at the same voltage. At these voltages however, both devices show breakdown characteristics, which is most evident by the reduction in luminous efficiency (Fig. 2b). As a result, a direct comparison of the devices at maximum luminance would not be practicable.

The luminance of the devices was therefore compared at lower voltages before the points at which the diodes begin to break down and the luminous efficiency begins to decrease. A luminance of 100 cdm^{-2} was chosen for comparison as this is similar to the brightness of an LCD screen. The Au grid TCE emits light with a luminance of 100 cdm^{-2} at a lower voltage than the ITO OLED (10.9 V compared 12.4 V), which reflects the fact that it has a lower turn-on voltage. At a comparative voltage, 10.9 V, the reference ITO OLED achieves a luminance of only 11.5 cdm^{-2}; 11.5% of the luminance of the Au grid TCE OLED at the same voltage.

A comparison of the luminance increase with increasing voltage in the region after turn-on, shows that the Au TCE and the ITO reference diodes produce equivalent amounts of light. The luminance vs. voltage curve gradient for the gold TCE OLED is 0.885 cdm^{-2}V^{-1} compared to 0.831 cdm^{-2}V^{-1} for the ITO OLED. The gold TCE therefore shows promise as a replacement for ITO in devices which require relatively low luminance such as in OLED display screens.

3.2. Electrical properties

3.2.1. Conduction mechanism

The IV data was analysed using various conduction models (see supplementary data), including electrode limited conduction effects (Schottky [22] and Fowler Nordheim [23,24]) and bulk limited conduction effects (Poole-Frenkel

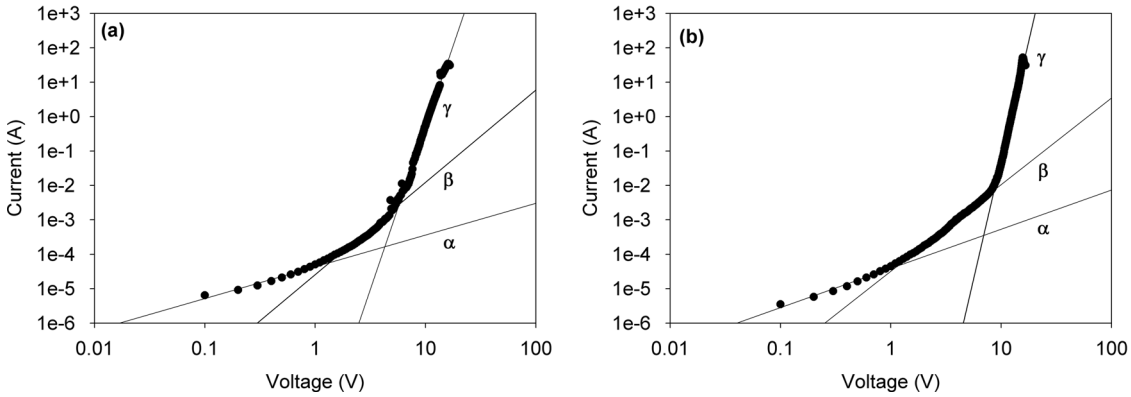

Figure 3 Conduction mechanism plot fit to I/V data for an OLED with (a) a gold grid TCE and (b) ITO. The solid lines labelled α, β and γ are linear fits to the data at low, mid-range and high voltage.

Table 1 Approximate relationship between current and voltage for the SCLC plots in Fig. 3.

	<1.28 V	1.28 > 5.65 V	>5.65 V
Au Grid TCE	$I \propto V$	$I \propto V^{2.7}$	$I \propto V^{9}$
	<1.18 V	1.18 > 8.45 V	>8.45 V
ITO	$I \propto V$	$I \propto V^{2.5}$	$I \propto V^{14}$

[25, 26] and space charge limited current [SCLC] [27]), to determine the limiting conduction method in the diodes and to see if this changed with the replacement of the ITO with the Au TCE.

The values of the relative permittivity of conducting polymers are typically between 2 and 12, [28] and the relative barrier heights between the materials in the diodes can be estimated by examination of the band diagrams (Fig. 2c). A combination of low relative permittivities (<2.0) and barrier heights (<0.5 eV) suggest that neither the Schottky nor Poole Frenkel conduction mechanisms are occurring in our diodes. Similarly, the barrier heights calculated from the Fowler Nordheim plots suggest this mechanism is not occurring.

In fact, the data is seen to follow a SCLC model (Fig. 3). The data obeys ohm's law, $J \propto V$ (slope α in Fig. 3), at low voltages, where the injected charge density is lower than the thermally generated carrier density. At higher voltages, the current becomes space-charge-limited with the modification due to the presence of the traps, and the slope of the graph increases to approximately $J \propto V^2$ (slope β in Fig. 3). At still higher voltages, the current increases rapidly over a small voltage range (slope γ in Fig. 3). The point at which this occurs is the trap filled limit, V_{TFL}. For the Au grid TCE, $V_{TFL} = 5.65$ V, and for the ITO, $V_{TFL} = 8.45$ V, reflecting the difference in turn-on voltages for the respective diodes (Fig. 2a). If trap-modified SCLC is occurring, the curve will continue on this slope until all the traps are filled, and the current returns to a trap-free situation where the curve returns to a $J \propto V^2$ relationship [22]. Approximate relationships between current and voltage are given in Table 1.

Although the assignment of the SCLC mechanism is not conclusive, because there is no evidence of a return to a $J \propto V^2$ character at high current values, the data suggests there is potentially a trap-modified SCLC mechanism occurring in our diodes. A number of polymer films, including thiophene based polymers, have previously been found to be space charge limited using ITO substrates as hole injectors [29–31]. The fact that the limiting conduction mechanism is not seen to change by the replacement of the ITO with the Au grid TCE, suggests that the Au grid is an acceptable ITO replacement technology when it comes to electrical conduction through the OLED.

3.2.2. Electrical charge generation and recombination

The conduction of charge in the gaps between the Au grid lines is expected to be poor, especially given the comparative resistivity of the polymer components of the OLED. For example, the measured sheet resistance of the PEDOT:PSS layer is $10^8\ \Omega\square^{-1}$. This suggests that holes will not diffuse very far in the PEDOT:PSS, and subsequently less holes are expected to be injected into the area of the emissive layer directly above the gaps in the grid lines (this is demonstrated by the Matlab simulation in Supplementary Materials which shows the field lines between the electrodes in the OLED). As there is no other conductive layer to help spread the holes uniformly before it enters the emissive layer, and as holes are less likely to travel through the higher resistance region of polymer, the regions of the emissive layer above the Au TCE gaps were not expected to emit as much light as the regions directly above the grid lines.

This was not the case as the emitted light was shown to be relatively uniform across the gap between the Au grid lines (Fig. 1c). Despite the high sheet resistance of PEDOT:PSS, holes injected from the Au grid collect at the PEDOT:PSS/F8BT interface where they face a significant energy barrier (Fig. 2c), and can be expected to distribute through the PEDOT:PSS layer [32]. Electrons are injected from the Al back electrode, transfer through the F8BT and recombine with holes at the PEDOT:PSS/F8BT interface.

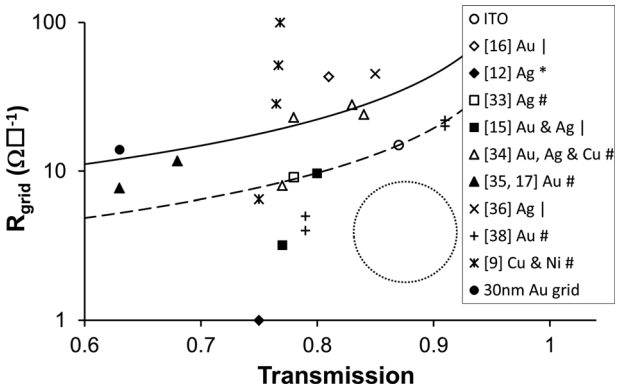

Figure 4 Plot of series resistance (R_s) vs. transmission for various metallic grid TCEs used in this work (•) and referenced in the literature. Experimental data is given for an Au grid with a line thickness of 30 nm. This is compared to a theoretical model of R_s vs. transmission for a line thickness of 100 nm (dashed line) and 40 nm (solid line) with varying line spacing and a constant line width of 3 μm. The area at the bottom right defined by the dotted circle defines the desired properties for an efficient TCE. Symbols used in legend for grid shape: | = lines, # = squares, * = hexagons. See Table S5 in Supporting Materials for details of grids used in each of the references.

The barrier to holes at this interface causes the charge carriers to spread out across the polymer layers, and to recombine distant from the electrodes. This in turn leads to emission of the light evenly across the polymer, and hence produces the uniform emission seen in the gaps between the Au grid lines.

The recombination may be aided by introducing a thin conducting layer between the TCE gaps (Fig. S3(b) in Supplementary Materials). This has the effect of spreading the field across the gaps more homogeneously and consequently improving the injection of charge from the Au grid electrode into the inter-electrode gaps. This may be achieved by using, for example, a thin conducting polymer layer, or a layer of conducting nanomaterial such as graphene, as long as the layer is sufficiently transparent to allow the generated light to escape from the diode.

3.2.3. Comparison of sheet resistance and transmission

The Au grid TCE has been further compared to previous work based on the main performance criteria for TCEs (low sheet resistance and high optical transmission). Besides metal grid TCEs, silver nanowire TCEs have previously been produced which have a sheet resistance, R_s, of 13 Ω□$^{-1}$ and a transmission of 85% at 550 nm, [10] while CNT films have been used with a reported sheet resistance of 30 Ω□$^{-1}$ and an average transmission of 70% throughout the visible wavelength range (400–700 nm) [8].

An examination of the series resistances (R_s) and transmissions of various metallic TCEs in the literature (Fig. 4) gives an idea of the progress towards the production of an "ideal" TCE with a transmission >90% and R_s <20 Ω□$^{-1}$, and puts our work with Au grid TCEs into context. The figure presents experimental data for our Au grid as well as other literature results, and compares them to a theoretical model describing R_s vs. transmission for Au grids of increasing line spacing with line thicknesses of 100 nm (dashed line) and 40 nm (solid line).

The theoretical model of R_s vs. transmission for a Au grid TCE is plotted by calculating the transmission of light through the grid and the sheet resistivity of the grid. The transmission of light through the grid, T_{total}, consists of the sum of the light transmitted through the metal and the light transmitted through the gaps in the Au grid, as:

$$T_{total} = \left(\left[A_{metal} . T_{metal} \right] + \left[\left(1 - A_{metal} \right) . T_{gap} \right] \right) T_{glass} \quad (1)$$

where, A_{metal} = fractional surface area covered by metal, T_{metal} = transmission through metal of given thickness, [37] T_{gap} = transmission through any material in the gaps between the Au grid (calculated from previous measurements), T_{glass} = transmission through glass (= 0.94).

Similarly, the sheet resistance of the grid, R_{grid}, can be estimated, where:

$$R_{grid} = \left(\frac{\left[R_{metal} / A_{metal} \right] \left[\left(R_{metal} l / w \right) + R_{gap} \right]}{\left[R_{metal} / A_{metal} \right] + \left[\left(R_{metal} l / w \right) + R_{gap} \right]} \right) \varepsilon \quad (2)$$

and,

$$R_{metal} = \rho_{metal} / d$$

where, R_{grid} = sheet resistance of grid, A_{metal} = fractional surface area covered by metal, R_{metal} = sheet resistance of metal, ρ = resistivity, d = metal thickness, l = length of metal lines, w = edge to edge distance of a hexagon cell, R_{gap} = sheet resistance of material in gaps e.g. PEDOT:PSS (measured). ε is an empirical factor to account for the fact that the deposited metal has a different resistivity to the bulk metal. Fitting the model to the experimental data gives $\varepsilon = 8$. Further information on the program used to model the OLED is given in the Supplementary Materials.

The experimental data presented for Au grid TCEs from this experiment and the literature is in good agreement with the theoretical model, where transmission increases but R_{grid} also increases as the Au TCE grid spacing increases or as the line thickness decreases. The trend described by the model suggests that a Au grid alone would be unable to achieve the desired TCE properties of transmission >90% and R_{grid} <20 Ω□$^{-1}$, and metal-based TCEs may require the incorporation of an additional transparent conducting element, such as a graphene layer [38], to achieve this.

4. Conclusions

ITO is currently the TCE of choice for use in OLEDs. Yet, it has several disadvantages, such as being brittle

and expensive, and its popularity has led to fears that it may become scarce. Here, a Au grid TCE was tested as a potential replacement for ITO in OLEDs, and the luminance characteristics of the Au TCE OLED are reported for the first time. An OLED, using a gold hexagonal grid as the TCE, was produced with the structure: glass/TCE/PEDOT:PSS/F8BT/BCP/Al. The OLED displayed performance comparable to a reference OLED incorporating an ITO electrode. The gold TCE OLED had a lower turn-on voltage, due to its lower work function, and lower operating voltages prior to breakdown. The Au grid TCE OLED displayed homogeneous light output through the areas between the grid lines, and showed comparable luminance with the ITO reference OLED at voltages lower than the breakdown voltage of the diodes. Importantly, the conduction mechanism (space charge limited current) does not change when the ITO is replaced by the Au grid TCE. This shows that a Au grid could potentially replace ITO in devices such as OLEDs.

The modelling completed here suggests that the sheet resistance and the transmission of the gold grid can be improved to lower the operating voltage and to increase the luminance of the OLED. The transmission can be increased by using larger line spacings, whilst maintaining the line width. The line thickness would have to increase to maintain a low sheet resistance, but a higher line thickness would increase the surface roughness, and this would require a thicker PEDOT:PSS to prevent short-circuits. This in turn would increase the operating voltage. In order to use thicker Au lines therefore, a way of planarising the grid surface may be advantageous.

A layer of conductive PEDOT:PSS or graphene [38] can be deposited on top of the grid structure to help spread the current across the gaps between the grid lines to improve the light emission through the gaps. This should increase the luminance of the OLED by both reducing the sheet resistance of the grid TCE for a given transmission, and also by increasing the light emission from the active layer. Such improvements in device architecture would be expected to move the TCE towards the ideal case of high transparency and low sheet resistance.

Supporting information for this article is available free of charge under http://dx.doi.org/10.1002/lpor.201300121

Received: 13 August 2013, **Revised:** 8 October 2013, **Accepted:** 29 October 2013

Published online: 27 November 2013

Key words: organic light emitting diodes, transparent conductors, ITO, metal grids.

References

[1] G. Haacke, Annu. Rev. Mater. Sci. **7**(1), 73–93 (1977).
[2] H. Kim, C. M. Gilmore, A. Pique, J. S. Horwitz, H. Mattoussi, H. Murata, Z. H. Kafafi, and D. B. Chrisey, J. Appl. Phys. **86**(11), 6451–6461 (1999).
[3] R. Paetzold, K. Heuser, D. Henseler, S. Roeger, G. Wittmann, and A. Winnacker, Appl. Phys. Lett. **82**(19), 3342–3344 (2003).
[4] L. Brand, "BRIEFING No. 26 Addressing critical commodity scarcity" (ObservatoryNANO, EU 2012).
[5] S. Choi, W. J. Potscavage and B. Kippelen, Opt. Express **18**(S3), A458–A466 (2010).
[6] J. R. Sheats and D. B. Roitman, Synthetic Met. **95**(2), 79–85 (1998).
[7] H. Aziz and Z. D. Popovic, Chem. Mater. **16**(23), 4522–4532 (2004).
[8] Z. Wu, Z. Chen, X. Du, J. M. Logan, J. Sippel, M. Nikolou, K. Kamaras, J. R. Reynolds, D. B. Tanner, A. F. Hebard, and A. G. Rinzler, Science **305**(5688), 1273–1276 (2004).
[9] D. S. Ghosh, T. L. Chen, and V. Pruneri, Appl. Phys. Lett. **96**(4), 041109 (2010).
[10] S. De, T. M. Higgins, P. E. Lyons, E. M. Doherty, P. N. Nirmalraj, W. J. Blau, J. J. Boland, and J. N. Coleman, ACS Nano **3**(7), 1767–1774 (2009).
[11] J.-Y. Lee, S. T. Connor, Y. Cui, and P. Peumans, Nano Lett. **8**(2), 689–692 (2008).
[12] Y. Galagan, J.-E. J. Rubingh, R. Andriessen, C.-C. Fan, P. W. Blom, S. C. Veenstra, and J. M. Kroon, Sol. Energ. Mat. Sol. C. **95**(5), 1339–1343 (2011).
[13] J.-S. Yu, I. Kim, J.-S. Kim, J. Jo, T. T. Larsen-Olsen, R. R. Søndergaard, M. Hösel, D. Angmo, M. Jørgensen, and F. C. Krebs, Nanoscale **4**, 6032–6040 (2012).
[14] A. Cheknane, Prog. Photovoltaics Res. Appl. **19**(2), 155–159 (2011).
[15] P. Kuang, J.-M. Park, W. Leung, R. C. Mahadevapuram, K. S. Nalwa, T.-G. Kim, S. Chaudhary, K.-M. Ho, and K. Constant, Adv. Mater. **23**(21), 2469–2473 (2011).
[16] W. Kubo and S. Fujikawa, J. Mater. Chem. **19**, 2154–2158 (2009).
[17] M.-G. Kang and L. Guo, Adv. Mater. **19**(10), 1391–1396 (2007).
[18] D. K. Schroder, Semiconductor Material and Device Characterization, 2nd Edition (Wiley-Interscience 1998).
[19] S. Haque, S. Koops, N. Tokmoldin, J. Durrant, and J. Huang, D. Bradley and E. Palomares Adv. Mater. **19**(5), 683–687 (2007).
[20] "Sigma-Aldrich chemical company (2013)," [Online]. Available: http://www.sigmaaldrich.com/catalog/product/aldrich/140910?lang = en&region = GB.
[21] T. Kietzke, D. Neher, M. Kumke, R. Montenegro, K. Landfester, and U. Scherf, Macromolecules **37**(13), 4882–4890 (2004).
[22] D. Taylor, IEEE T Dielect. El. In. **13**(5), 1063–1073, Oct.
[23] I. D. Parker, J. Appl. Phys. **75**(3), 1656–1666 (1994).
[24] R. H. Fowler and L. Nordheim, P. Roy. Soc. Lond. A **119**(781), 173–181 (1928).
[25] S. V. Rakhmanova and E. M. Conwell, Appl. Phys. Lett. **76**(25), 3822–3824 (2000).
[26] J. Frenkel, Phys. Rev. **54**, 647–648 (1938).
[27] M. A. Lampert, Phys. Rev. **103**, 1648–1656 (1956).
[28] Q.-D. Ling, D.-J. Liaw, C. Zhu, D. S.-H. Chan, E.-T. Kang, and K.-G. Neoh, Prog. Polym. Sci. **33**(10), 917–978 (2008).

[29] P. W. M. Blom, M. J. M. d. Jong, and J. J. M. Vleggar, Appl. Phys. Lett. **68**(23), 3308–3310 (1996).
[30] I. Musa, W. Eccleston, and S. J. Higgins, J. Appl. Phys. **83**(10), 5558–5560 (1998).
[31] I. Musa, S. J. Higgins, and W. Eccleston, J. Appl. Phys. **81**(5), 2288–2290 (1997).
[32] L. S. C. Pingree, B. A. MacLeod, and D. S. Ginger, J. Phys. Chem. C **112**, 7922–7927 (2008).
[33] J. Zou, H.-L. Yip, S. K. Hau, and A. K.-Y. Jen, Appl. Phys. Lett. **96**(20), 203301 (2010).
[34] M.-G. Kang, M.-S. Kim, J. Kim, and L. J. Guo, Adv. Mater. **20**(23), 4408–4413 (2008).
[35] D. S. Hecht, L. Hu, and G. Irvin, Adv. Mater. **23**(13), 1482–1513 (2011).
[36] K. Tvingstedt and O. Inganäs, Adv. Mater. **19**(19), 2893–2897 (2007).
[37] E. Palik (ed.) Handbook of Optical Constants of Solids (Academic Press 1985).
[38] Y. Zhu, Z. Sun, Z. Yan, Z. Jin, and J. M. Tour, ACS Nano **5**(8), 6472–6479 (2011).